Charge transfer in time-dependent density-functional theory: Insights from the asymmetric Hubbard dimer

J. I. Fuks and N. T. Maitra

Department of Physics and Astronomy, Hunter College and the City University of New York, 695 Park Avenue, New York, New York 10065, USA

(Received 22 December 2013; revised manuscript received 14 April 2014; published 5 June 2014)

We show that propagation with the best possible adiabatic approximation in time-dependent density-functional theory fails to properly transfer charge in an asymmetric two-site Hubbard model when beginning in the ground state. The approximation is adiabatic but exact otherwise, constructed from the exact ground-state exchange-correlation functional that we compute via constrained search. The model shares the essential features of charge-transfer dynamics in a real-space long-range molecule, so the results imply that the best possible adiabatic approximation, despite being able to capture nonlocal ground-state step features relevant to dissociation and charge-transfer excitations, cannot capture fully time-resolved charge-transfer dynamics out of the ground state.

DOI: 10.1103/PhysRevA.89.062502 PACS number(s): 31.15.ee, 71.15.Mb, 71.10.Fd

I. INTRODUCTION

Charge-transfer (CT) dynamics are increasingly important in biology, chemistry and physics, underlying critical processes in photovoltaics, vision, photosynthesis, molecular electronics, and the control of coupled electron-ion dynamics (see, e.g., Refs. [1–5]). Yet an accurate theoretical description, capturing correlated electron motion, is notoriously difficult especially over large distances. For most applications, a time-resolved picture is crucial, and the systems are large enough that time-dependent density-functional theory (TDDFT) is the only calculationally feasible approach [6–8]. Standard functional approximations underestimate CT excitations, but improved functionals have been developed [9]. Still, a truly time-resolved description must go beyond a calculation of the excitation spectrum: electron transfer between regions of space is clearly nonperturbative. TDDFT certainly applies in the nonlinear regime and has given useful predictions in many cases, including CT dynamics [10]. At the same time, there is a dearth of alternative accurate practical methods to test TDDFT calculations. Results on simplified exactly solvable model systems are not always optimistic [11–14].

Almost all nonperturbative TDDFT calculations utilize an adiabatic exchange-correlation potential: $v_{\rm XC}^{\rm A}[n;\Psi_0,\Phi_0](\mathbf{r},t) = v_{\rm XC}^{\rm g.s.}[n(t)](\mathbf{r})$. Errors arise from two distinct sources: one is the choice of the ground-state (g.s.) functional approximation, the other is the adiabatic approximation itself. To separate these the *adiabatically exact* (AE) approximation [15] is defined: the instantaneous density is input into the exact g.s. functional, $v_{\rm XC}^{\rm AE}[n;\Psi_0,\Phi_0](\mathbf{r},t) = v_{\rm XC}^{\rm AE}[n](\mathbf{r},t) = v_{\rm XC}^{\rm exact\ g.s.}[n(t)](\mathbf{r})$. This approximation neglects memory effects (dependence on the density's history and true and Kohn–Sham initial states Ψ_0 and Φ_0) but is fully nonlocal in space. Finding $v_{\rm XC}^{\rm AE}[n](\mathbf{r},t)$ requires an iterative density-inversion scheme to find interacting and noninteracting g.s.'s of a given density, and it has been done just for a few model systems [13–15]. Usually one evaluates the AE potential on the exact density $n(t)$, $v_{\rm XC}^{\rm AE}[n(t)](\mathbf{r})$, and compares with the exact potential $v_{\rm XC}[n,\Psi_0,\Phi_0](\mathbf{r},t)$ at that time to analyze how good the approximation is. A more useful assessment however, would be to self-consistently propagate the Kohn–Sham (KS) orbitals with it, using at each time step the AE potential evaluated on the self-consistent instantaneous density. This clearly requires much more numerical effort, because many iterations need to be performed at every time step to find the potential to propagate in; it has only been done in a few examples [15–17]. For CT it is particularly challenging to converge the iterations, due to the very low density between the atoms.

For a model molecule composed of closed-shell atoms and driven at the CT resonance, a step associated with the CT process gradually builds up over time in the exact correlation potential [14]. The AE approximation fails to capture the dynamical step of Refs. [13,18] but, when evaluated on the *exact* density, does show a CT step, although of a smaller size than the exact. Available approximations do not yield any step structure whatsoever, and the dismal failure of several adiabatic functionals to transfer any charge was shown in Refs. [14,19]. We expect some blame must go to the adiabatic approximation itself, but is the partial step of the AE approximation enough to give a reasonable description of the CT dynamics? If yes, this would greatly simplify the ongoing search for accurate functionals for nonperturbative CT. To answer the question, we must propagate with the AE self-consistently but, as discussed above, this procedure is numerically very challenging for CT dynamics. We show here that the answer is no, by studying CT in a two-fermion asymmetric Hubbard dimer, which shares the essential features of CT dynamics in real-space molecules. Due to the small Hilbert space of the dimer the exact g.s. functional can be found and used in $v_{\rm XC}^{\rm AE}(t)$ to self-consistently propagate the system. We can then assess errors in the adiabatic approximation for CT dynamics independently of those due to the g.s. approximation used. We find the adiabatic approximation is inherently poor and analyze the potentials to explain why.

II. THE ASYMMETRIC HUBBARD MODEL

The Hamiltonian of the two-site interacting Hubbard model with on-site repulsion U and hopping parameter T [20–27] is

$$\hat{H} = -T\sum_{\sigma}(\hat{c}_{L\sigma}^{\dagger}\hat{c}_{R\sigma} + \hat{c}_{R\sigma}^{\dagger}\hat{c}_{L\sigma}) + U(\hat{n}_{L\uparrow}\hat{n}_{L\downarrow} + \hat{n}_{R\uparrow}\hat{n}_{R\downarrow}) + \frac{\Delta v(t)}{2}(\hat{n}_L - \hat{n}_R), \quad (1)$$

where $\hat{c}_{L(R)\sigma}^{\dagger}$ and $\hat{c}_{L(R)\sigma}$ are creation and annihilation operators for a spin-σ electron on the left (right) site L (R), respectively,

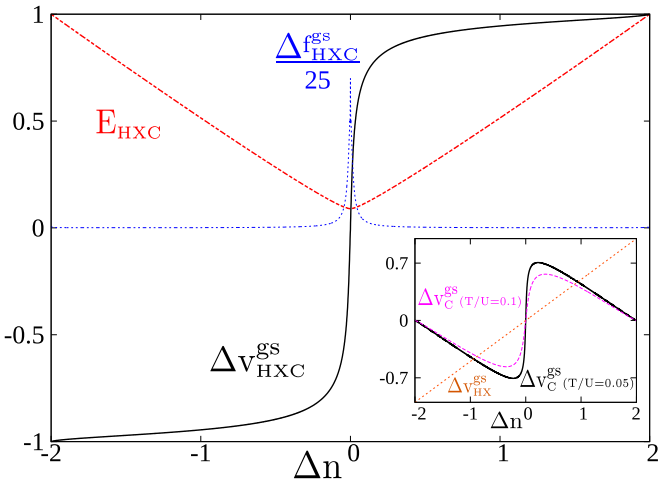

FIG. 1. (Color online) Exact $E_{\rm HXC}[\Delta n]$ (red dashed), g.s. potential $\Delta v^{\rm g.s.}_{\rm HXC}[\Delta n]$ (black solid), and scaled g.s. kernel $\Delta f^{\rm g.s.}_{\rm HXC}[\Delta n]/25$ (blue dotted) for $T/U = 0.05$. The inset shows the correlation potential $\Delta v^{\rm g.s.}_{\rm C}[\Delta n]$ for $T/U = 0.05$ (black solid), $T/U = 0.1$ (pink dashed), and the HX potential $\Delta v^{\rm g.s.}_{\rm HX}[\Delta n]$ (independent of T, orange dotted). All functionals are in units of U.

and $\hat{n}_L = \sum_{\sigma=\uparrow,\downarrow} \hat{c}^\dagger_{L\sigma}\hat{c}_{L\sigma}$ and $\hat{n}_R = \sum_{\sigma=\uparrow,\downarrow} \hat{c}^\dagger_{R\sigma}\hat{c}_{R\sigma}$ are the site-occupancy operators. The dipole $\langle \hat{n}_L - \hat{n}_R \rangle = \Delta n$ is the main variable [25]; the total number of fermions is fixed at two. A static potential between the sites, $\Delta v^0 = \sum_\sigma (v^0_{L\sigma} - v^0_{R\sigma})$, renders the Hubbard dimer asymmetric. The external potential $\Delta v(t)$ is given by $\Delta v(t) = \Delta v^0 + 2\mathcal{E}(t)$. The long-range molecule is modeled by $T/U \to 0$: for fixed U, $T \to 0$ corresponds to a large separation between the sites (equivalent to the strongly correlated limit $U \to \infty$). We choose $T = 0.05$, use $\hbar = e = 1$ throughout, and energies are given in units of U.

The singlet sector of the vector space is three-dimensional, enabling an exhaustive search over all wave functions to find the exact Hartree-exchange-correlation (HXC) energy functional, $E_{\rm HXC}[\Delta n]$, plotted in Fig. 1. This follows the procedure of Ref. [25].

As T/U decreases the energy becomes sharper at $\Delta n = 0$ (Fig. 1), while the potential $\Delta v^{\rm g.s.}_{\rm HXC}[\Delta n]$ approaches a step function there, contained in the correlation potential (see inset of Fig. 1). This indicates the derivative discontinuity of the one-electron site, as will be discussed shortly. Note that $\Delta v_{\rm HXC} = \Delta v_{\rm HX} + \Delta v_{\rm C}$ where $\Delta v_{\rm HX} = U\Delta n/2$ [25].

The KS Hamiltonian has the form of Eq. (1) but with $U = 0$ and $\Delta v(t)$ replaced by $\Delta v_{\rm S}[\Delta n, \Phi_{\rm g.s.}](t) = v_{\rm HXC}[\Delta n, \Psi_{\rm g.s.}, \Phi_{\rm g.s.}](t) + \Delta v(t)$, defined such that the interacting density $\Delta n(t)$ is reproduced. A self-developed code in second quantization, using a Crank–Nicolson propagator and a 0.01 time step, was used for the propagations.

To model closed-shell to closed-shell (cs-cs) CT in a real molecule, we focus on the $\Delta v^0 = -2.0U$ problem where the g.s. has $\Delta n_{\rm g.s.} = 1.9901$ and study the transition to the CT excited state with $\Delta n_{\rm CT} = 0.0090$ and frequency $\omega_{\rm CT} = 1.0083U$; we take $\mathcal{E}(t) = 0.1\sin(1.0083Ut)U$. For open-shell to open-shell (os-os) CT in a real molecule, we instead take $\Delta v^0 = -0.4U$, resulting in a slightly asymmetric g.s. $\Delta n_{\rm g.s.} = 0.021\,37$, and study the transition to the CT excited state where $\Delta n_{\rm CT} = 1.9734$ and $\omega_{\rm CT} = 0.6199U$; here we take $\mathcal{E}(t) = 0.09\sin(0.6199Ut)U$. In either case the field $\mathcal{E}(t)$ is resonant with magnitude weak enough such that only the ground and above-mentioned CT states are significantly occupied during the dynamics. We also will briefly consider the results of propagation under different static potential differences and under detuned conditions.

A. Closed-shell to closed-shell charge transfer

The dipoles are shown on the left panel of Fig. 2; the CT excited state is reached at around $t = 224/U$. The similarity of the exact dipole with the real-space dynamics of Fig. 4 of Ref. [14] and the CIS/CISD dynamics of Figs. 3 and 4 of Ref. [19] is evident; also the adiabatic exact-exchange (AEXX) dipole on the left of Fig. 2 drastically fails to complete the CT, resembling the real-space AEXX and HF cases. Propagating the KS system with the AE functional, obtained at each time step by inserting the instantaneous density $\Delta n^{\rm AE}_{sc}$ into the exact g.s. HXC potential $\Delta v^{\rm g.s.}_{\rm HXC}[\Delta n^{\rm AE}_{sc}]$ of Fig. 1, we obtain $\Delta n^{\rm AE}_{sc}$ on the left of Fig. 2. $\Delta n^{\rm AE}_{sc}$ follows the exact for a longer time than the AEXX but ultimately fails to complete the CT.

In Fig. 3 the exact and AE dipole moments for the cs-cs CT problem for different values of the external potential $\Delta v(t)$ and detuning are shown. In the left panel we show the results of resonant dynamics for different static potential differences Δv^0. The breakdown of the adiabatic approximation occurs in a similar way in all cases, with the AE dipole following the exact for some period of time but then turning back towards the ground-state value before much charge transfer occurs. The time that the AE dipole begins to deviate from the exact is earlier in the Rabi cycle for larger $|\Delta v^0|$ (which has a larger CT resonant frequency) although the absolute value of this time is later since the Rabi period is also greater for greater $|\Delta v^0|$.

In the right panel of Fig. 3 the static potential difference is kept fixed at $\Delta v^0 = -2.0U$ but the frequency ω of the applied laser, $\mathcal{E}(t) = 0.1\sin(\omega t)U$, is varied. In the upper panel the laser is resonant $\omega = \omega_{\rm CT}$, whereas the lower panels show the results for detuned Rabi oscillations. Note that for the chosen parameters, the AE linear response resonance is only shifted by 0.001 U from the interacting resonance $\omega_{\rm CT}$ [28]. Interestingly the AE propagation shows an increased amount of transferred charge in the detuned cases. We conclude from these graphs that the performance of adiabatic TDDFT is also poor to describe off-resonant CT. The AE propagation shows that one must go beyond the adiabatic approximation to correctly describe CT when beginning in the ground state.

We next consider the behavior of the HXC potentials. The exact and AE potentials are shown on the left of Fig. 4. The top-left panel shows the exact KS potential alongside the applied field. The middle-left panel shows the exact HXC potential $\Delta v_{\rm HXC}[\Delta n](t)$, the AE potential evaluated on the exact density $\Delta v^{\rm AE}_{\rm HXC}[\Delta n](t)$, and the AE potential evaluated on the self-consistent density $\Delta v^{\rm AE}_{\rm HXC}[\Delta n^{\rm AE}_{sc}](t)$. The exact $\Delta v_{\rm HXC}[\Delta n](t)$ is found by inserting the exact density $\Delta n(t)$ into [21,24]

$$\Delta v_{\rm HXC}[\Delta n] = -\frac{\ddot{\Delta n} + 4T^2\Delta n}{\sqrt{4T^2(4-\Delta n^2) - \dot{\Delta n}^2}} - \Delta v^0 - 2\mathcal{E}(t), \quad (2)$$

This starts at its g.s. value $\Delta v_{\rm HXC}[\Delta n^0 = 1.9901, \dot{\Delta n} = \ddot{\Delta n} = 0] \approx 1$ but soon increases sharply and makes very large

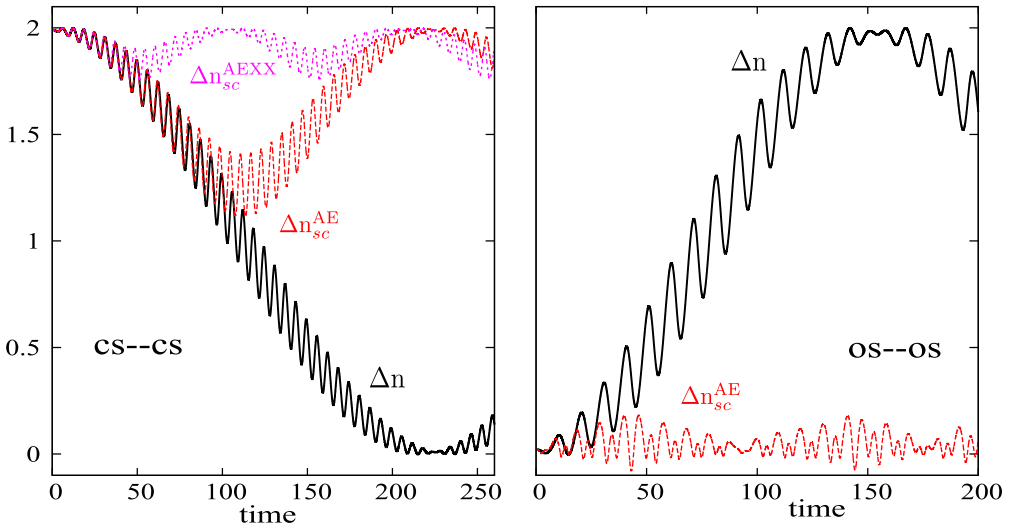

FIG. 2. (Color online) Exact dipole Δn (black solid), AE dipole $\Delta n_{sc}^{\mathrm{AE}}$ (red dashed), and the AEXX dipole $\Delta n_{sc}^{\mathrm{AEXX}}$ (pink dotted). Left panel is for cs-cs CT. Right panel is for os-os CT. Time is in units of $1/U$.

oscillations, which appear to be related to maintaining noninteracting v-representability [21,24,26,28]: at the times of the first sharp changes, the denominator in the first term of Eq. (2) approaches zero, and the direction of the sharp potential change is such to prevent the denominator from actually becoming zero. Averaging through the oscillations, we see that the exact Δv_{HXC} goes to $-\Delta v^0$ at $t \approx 224/U$, i.e., the exact Δv_{S} becomes zero, aligning the two sites (top panel). This is completely analogous with the real-space case: there, a step in the HXC potential in the intermolecular region develops such that when the CT state is reached, the atomic levels of the donor (D) ion and acceptor (A) ion are "realigned," i.e., the step has size $|I_D^{N_D-1} - I_A^{N_A+1}|$ in the large-separation limit [14]. In both real-space and Hubbard cases, it is the correlation potential (lower-left panel of Fig. 4) that contains this feature. The oscillations in the exact Δv_{HXC} around its average value near when the excited CT state is reached almost exactly cancel the oscillations in the external field, as reflected in the decreasing oscillations in the KS potential shown. This field-counteracting effect is a feature of the correlation potential. In the real-space case this effect is related to the absence of polarization due to truncation to a few-level system [13,18].

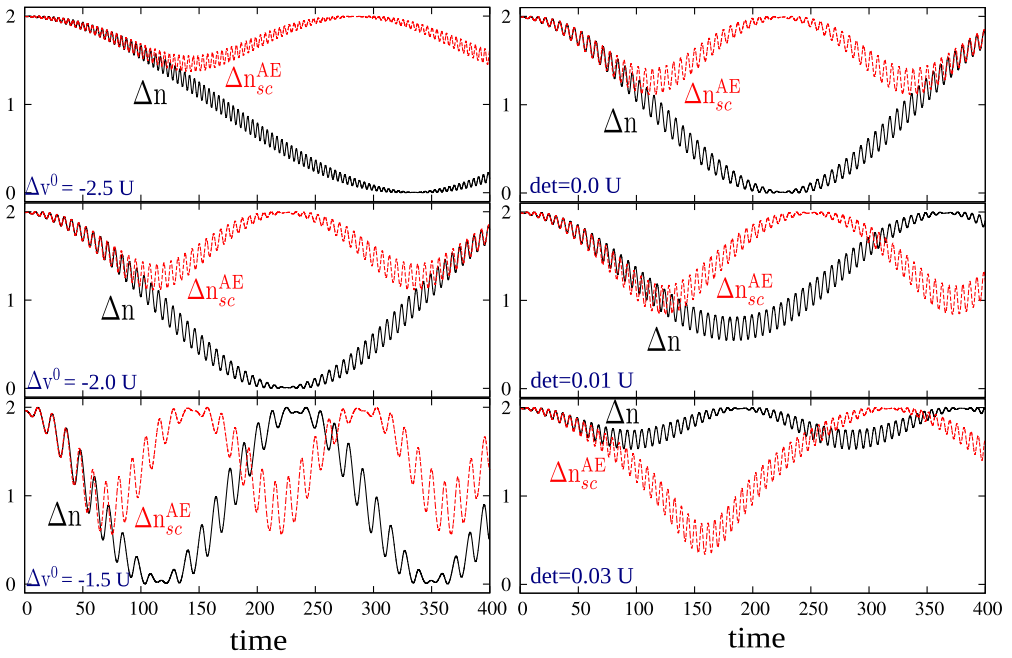

FIG. 3. (Color online) Left panel: Exact dipole Δn (black solid) and AE dipole $\Delta n_{sc}^{\mathrm{AE}}$ (red dashed) for different values of the static potential difference Δv^0 and resonant driving. Right panel: Same quantities but for fixed value of the static potential $\Delta v^0 = -2.0U$ and different detunings $\omega_{\mathrm{det}} = \omega - \omega_{\mathrm{CT}}$ of the laser frequency ω with respect to the interacting resonance $\omega_{\mathrm{CT}} = 1.0083U$. In all cases the amplitude of the laser is $0.1U$. Time is in units of $1/U$.

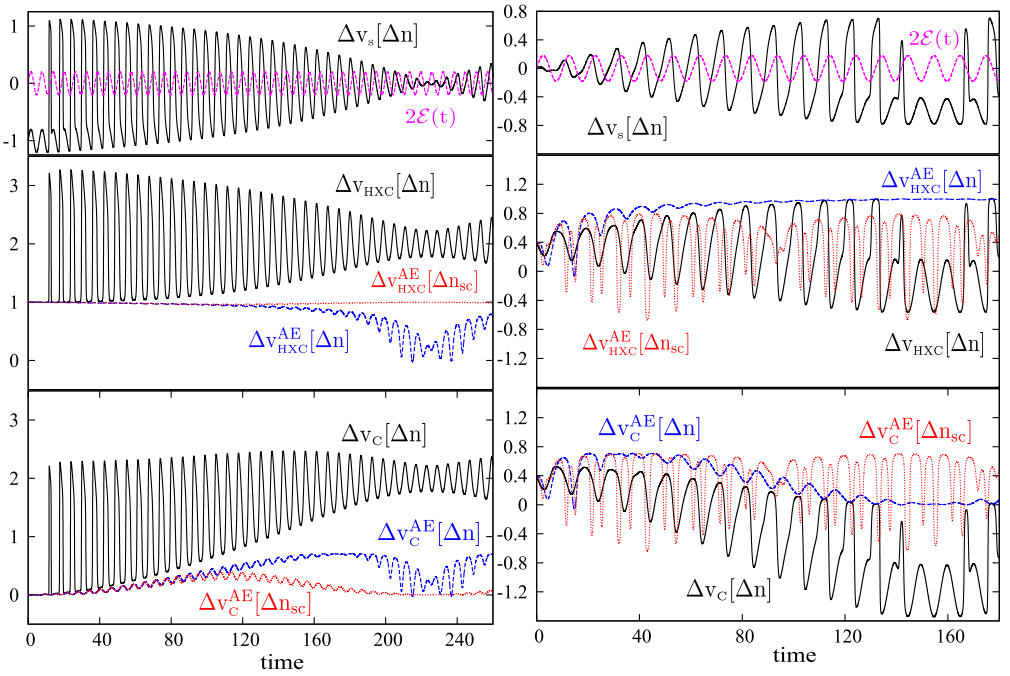

FIG. 4. (Color online) (Upper panel) Exact KS potential Δv_S [black solid; first term on right-hand side of Eq. (2)] and the field $\mathcal{E}(t)$ (pink dashed). (Middle panel) Exact HXC potential Eq. (2) (black solid), the AE HXC potential $\Delta v^{AE}_{HXC}[\Delta n]$ (blue dashed), and the AE HXC potential $\Delta v^{AE}_{HXC}[\Delta n_{sc}]$ (red dotted) with self-consistent $\Delta n_{sc} = \Delta n^{AE}_{sc}$. (Lower panel) Correlation potentials. The left panels show cs-cs CT. The right panels show os-os CT. Time is in units of $1/U$.

We now turn to the AE potentials. Consider first $\Delta v^{AE}_{HXC}[\Delta n](t)$. In the real-space case of Ref. [14], as the CT state is reached, the analogous AE correlation potential developed a step whose size, in the limit of large separation, approached $\Delta^D_c(N-1) \equiv I^{N-1}_D - A^{N-1}_D$, the derivative discontinuity of the $(N-1)$-electron donor. The same occurs in the Hubbard model. First observe that $\Delta v^{AE}_{HXC}[\Delta n](t)$ shown in Fig. 4 can be obtained by simply reading off the potential from Fig. 1, using the exact instantaneous value of $\Delta n(t)$ of Fig. 2. So the shape of $\Delta v^{AE}_{HXC}[\Delta n](t)$ just tracks that of the $\Delta v^{g.s.}_{HXC}$ curve of Fig. 1, moving from right to the center, gently oscillating around it. Now, Δn plays the role of the density variable as well as directly giving the particle number on each site, $n_{L,R} = 1 \pm \frac{\Delta n}{2}$. As a consequence, in the isolated-site limit $T/U \to 0$, a variation δn near $\Delta n = 0$ can be thought of as adding (subtracting) a fraction of charge δn to the one-fermion site on the left (right):

$$2\frac{dE_C[\Delta n]}{d(\Delta n)}\bigg|_{\Delta n=0^+} - 2\frac{dE_C[\Delta n]}{d(\Delta n)}\bigg|_{\Delta n=0^-} = \Delta v^{g.s.}_C[\Delta n = 0^+] - \Delta v^{g.s.}_C[\Delta n = 0^-] \equiv 2\Delta^{1\ site}_C(N=1), \tag{3}$$

where $E_C = E_{HXC} - \frac{U}{8}(4 + \Delta n^2)$ [25,27]. The difference in the correlation potential on either side of $\Delta n = 0$ therefore coincides with the derivative discontinuity of the one site with $(N-1)$ electrons. From Fig. 1, this approaches the value $\Delta^{1\ site}_C(N=1) \approx 0.7$ for $T/U = 0.05$. Returning to Fig. 4, as we approach the CT state $\Delta n_{CT} \to 0$, the exact $\Delta v_C[\Delta n]$ approaches $-\Delta v^0$ such that $\Delta v_S \to 0$ and the levels of the two sites get aligned; instead, the $\Delta v^{AE}_C[\Delta n]$ approaches $-\Delta v^{AE}[\Delta n_{CT}]$, i.e., the potential difference for which Δn_{CT} is a ground state. $\Delta v^{AE}_C[\Delta n]$ thus tracks the approaching discontinuity in Fig. 1; as $T/U \to 0$, this change becomes sharper and larger, occurring over an ever smaller region. Note that the factor 2 on the right of Eq. (3) results from expressing the energy functional in terms of the variable $\Delta n = n_L - n_R$, i.e.,

$$\Delta v_C[\Delta n] = v^L_C[\Delta n] - v^R_C[\Delta n] = \frac{dE_C[\Delta n]}{d(\Delta n)}\frac{d\Delta n}{dn_L} - \frac{dE_C[\Delta n]}{d(\Delta n)}\frac{d\Delta n}{dn_R}.$$

So, in the limit, in both the real-space molecule and the Hubbard dimer, the AE correlation potential in the CT state shifts the donor upwards relative to the acceptor by an amount equal to the derivative discontinuity of the $(N-1)$-electron donor; in both cases, this underestimates the shift provided by the exact correlation potential.

We now turn to $\Delta v^{AE}_{HXC}[\Delta n_{sc}](t)$ and $\Delta v^{AE}_C[\Delta n_{sc}](t)$ in Fig. 4. Initially, $\Delta v^{AE}_{HXC}[\Delta n_{sc}](t)$ follows the exact potential but very soon deviates from it: it makes small oscillations near its initial value, hardly noticeable on the scale of the changes of the exact $\Delta v_{HXC}[\Delta n](t)$. The dipole Δn^{AE}_{sc} is affected significantly only later (red dashed line on left side of Fig. 2); the relatively large external potential seems to carry the dipole oscillations with it for a while, before the effect of the incorrect correlation potential is felt. Certainly, the two sites never get anywhere close to being realigned; *a stable CT state that has one electron on each therefore cannot be approached*.

Finally, we note that the failure to transfer the charge is *not* due to the error that the AE approximation makes for the CT excitation energy. In fact, as shown in Ref. [28] $\omega^{AE} \approx \omega_{CT}$.

Reproducing accurately the excitation spectrum is not enough for a functional to be able to model time-resolved resonant CT dynamics.

B. Open-shell to open-shell charge transfer

The os-os AE dipole fails miserably even after a very short time, as shown in the right panel of Fig. 2; one electron more or less always hovers on each site, while the exact propagation reaches the CT state at about $153/U$. The KS, HXC, and correlation potentials are shown on the right-hand side of Fig. 4. The initial exact $\Delta v_{\rm C}(t=0)$ precisely cancels the static external potential: $\Delta v_{\rm S}(t=0)$ aligns the two sites, completely analogous to the real-space case, where the correlation potential of a heteroatomic diatomic molecule has a step that aligns the highest-occupied molecular orbital (HOMO) energies on each atom [29–31]. As charge transfers, the exact $\Delta v_{\rm S}(t)$ starts to oscillate on the optical scale, and there is a drop soon before the CT excitation is reached. The drop is related to the denominator of $\Delta v_{\rm S}(t)$ approaching zero as discussed before; in fact, the shape resembles that of the cs-cs starting at the CT excited state. The value of the exact $\Delta v_{\rm HXC}[\Delta n_{\rm CT}]$ can be obtained by taking $\dot{\Delta n} = \ddot{\Delta n} = 0$ in Eq. (2); note that it is different from that obtained from its AE counterpart $\Delta v_{\rm HXC}^{\rm AE}[\Delta n = 1.9734]$ (middle-right panel in Fig. 4). This reflects the fact that the exact state is an excited state, not a g.s. of any potential.

The AE potential starts correctly, as it should for ground states, capturing the alignment of the two sites, just as in the real-space case where $v_{\rm C}^{\rm AE}(\mathbf{r})$ captures the initial intermolecular step. However, $\Delta v_{\rm HXC}^{\rm AE}[n_{sc}](t)$ rapidly becomes a poor approximation, hardly resembling the exact at all. The site alignment creates a near degeneracy in the KS g.s., unlike in the interacting system. The true interacting system has a Heitler–London form in the g.s. and the CT excited state has a finite frequency. This vanishing of the KS gap implies that strong nonadiabaticity is required to open the gap to the finite one of the interacting system [32]: double-excitations are near-degenerate and critical to incorporate, and nonadiabaticity is required. The nature of the states and arguments above are the same as the real-space case, and so we expect that, also for real molecules, a self-consistent AE propagation will lead to a very poor dipole. As for $\Delta v_{\rm HXC}^{\rm AE}[\Delta n](t)$, it tracks $v_{\rm HXC}^{\rm g.s.}[\Delta n(t)]$ of Fig. 1 moving from near the center out to the right, with gentle oscillations reflecting the oscillations in $\Delta n(t)$. Again we note that its value when the CT state is reached is the HXC potential of a g.s. of density $\Delta n = 1.9734$ as opposed to the exact HXC potential which is that for an excited state of the same density.

A further similarity can be drawn between the real-space and Hubbard models considering the static HXC kernel, $\Delta f_{\rm HXC}^{\rm g.s.}[\Delta n] = d^2 E_{\rm HXC}[\Delta n]/d(\Delta n)^2$ (Fig. 1). The sharp-peaked structure at $\Delta n = 0$ becomes proportional to a δ function in the $T/U \to 0$ limit. The static kernel for real os-os molecules at large separation [33,34] also diverges. The exact nonadiabatic kernel $\Delta f_{\rm HXC}[\Delta n](\omega)$ must also diverge to open the gap, but there is a large nonadiabatic correction to the static kernel in this case, and the AE frequencies are significantly different from those of the true system [28].

III. CONCLUDING REMARKS

In both cases of CT presented, the form of the interacting state undergoes a fundamental change: in the cs-cs case, from approximately a single Slater determinant initially to two determinants of Heitler–London type in the CT state, while the reverse occurs for the os-os case. The KS state, however, always remains a single determinant. This gives the underlying reason for the development or loss of the CT step structure in the exact potential in real-space; the step is reflected in the Hubbard model by the realignment of the two sites, signifying strong correlation. An AE approximation captures this strong correlation effect perfectly when it occurs in the g.s. (os-os case), but even so our results show it fails to propagate well even at short times due to the near degeneracy in the KS system. In the cs-cs case, on the other hand, the AE propagation begins accurately but ultimately fails to develop the needed shift between donor and acceptor. The failure to charge transfer seen here and in the previous works [14,19] holds for the case where the charge transfer occurs from the ground state, either of a molecule consisting of closed-shell fragments, or consisting of open-shell fragments, and where the system undergoes the fundamental change to open-shell fragments in the first case and closed-shell fragments in the second case, once the CT excited state is reached. If, instead, the charge-transfer occurs from an already-excited state, for example, as modelled by the computation in Ref. [10] where the initial state is the photoexcited carotenoid triad, the situation is quite different, since there is not necessarily the fundamental change in the form of the interacting state described above. For example, in the case of closed-shell fragments, an initial local excitation on one fragment breaks the double occupation of the HOMO on the donor and, if the KS initial state is chosen appropriately, it could more naturally model the transfer of one electron from the donor to the acceptor, reducing the correlation effects. What the significance of nonadiabatic effects is in this case remains to be explored, including the generic "dynamical step" of nonlinear dynamics [13], but the analysis above suggests results of an adiabatic propagation might be better, given there is not as great a fundamental change in the form of the interacting state.

In summary, the asymmetric Hubbard dimer captures essential elements of CT dynamics across a real-space molecule, enabling a decisive verdict on the adiabatic approximation for time-resolved long-range CT dynamics. While previous work has shown the drastic performance of the usual adiabatic approximations [14,19], the present work shows that even propagating with the *best possible adiabatic* approximation, i.e., adiabatically exact, fails when modeling charge transfer beginning in the ground state, both in the resonant and in slightly-off-resonant cases. Accurately reproducing the CT frequency is not enough to model fully time-resolved CT. This suggests an urgent need to develop nonadiabatic approximations for CT dynamics. The step feature in the correlation potential, with nonlocal dependence on the density in both space and time, must be modeled; improved ground-state functionals are not adequate. The decomposition of the exact exchange-correlation potential into kinetic and interaction components [18] may offer a starting point for developing such nonadiabatic approximations and will be explored in our future work. Finally, we note that, clearly, there are aspects

of CT in real molecules not captured by our model: the effect of many electrons, three dimensions, and coupling to ionic motion. These likely buffer the impact of the step; however, there is no reason to expect it will still not have significant consequences. This hypothesis is supported by similar failures found when modeling time-resolved CT within adiabatic TDDFT in three-dimensional molecules [19].

ACKNOWLEDGMENTS

J.I.F. thanks Jordi Salvado and Mehdi Farzanehpour for useful conversations. We gratefully acknowledge financial support from the National Science Foundation CHE-1152784 (NTM) and the US Department of Energy Office of Basic Energy Sciences, Division of Chemical Sciences, Geosciences, and Biosciences under Award DE-SC0008623 (J.I.F.).

[1] W. R. Duncan and O. V. Prezhdo, Annu. Rev. Phys. Chem. **58**, 143 (2007).
[2] A. E. Jailaubekov *et al.*, Nat. Mater. **12**, 66 (2012).
[3] D. Polli *et al.*, Nature (London) **467**, 440 (2010).
[4] A. Nitzan and M. A. Ratner, Science **300**, 1384 (2003).
[5] G. Sansone *et al.*, Nature (London) **465**, 763 (2010).
[6] E. Runge and E. K. U. Gross, Phys. Rev. Lett. **52**, 997 (1984).
[7] *Fundamentals of Time-Dependent Density Functional Theory*, Lecture Notes in Physics Vol. 837, edited by M. A. L. Marques, N. T. Maitra, F. Nogueira, E. K. U. Gross, and A. Rubio, (Springer, Berlin, Heidelberg, 2012).
[8] C. A. Ullrich, *Time-dependent Density-Functional Theory* (Oxford University Press, Oxford, 2012).
[9] T. Stein, L. Kronik, and R. Baer, J. Am. Chem. Soc. **131**, 2818 (2009); R. Baer. E. Livshitz, and U. Salzner, Annu. Rev. Phys. Chem. **61**, 85 (2010).
[10] C. A. Rozzi *et al.*, Nat. Commun. **4**, 1602 (2013).
[11] M. Ruggenthaler and D. Bauer, Phys. Rev. Lett. **102**, 233001 (2009).
[12] J. I. Fuks, N. Helbig, I. V. Tokatly, and A. Rubio, Phys. Rev. B **84**, 075107 (2011).
[13] P. Elliott, J. I. Fuks, A. Rubio, and N. T. Maitra, Phys. Rev. Lett. **109**, 266404 (2012).
[14] J. I. Fuks, P. Elliott, A. Rubio, and N. T. Maitra, J. Phys. Chem. Lett. **4**, 735 (2013).
[15] M. Thiele, E. K. U. Gross, and S. Kümmel, Phys. Rev. Lett. **100**, 153004 (2008).
[16] M. Thiele and S. Kümmel, Phys. Rev. A **79**, 052503 (2009).
[17] R. Requist and O. Pankratov, Phys. Rev. A **81**, 042519 (2010).
[18] K. Luo *et al.*, J. Chem. Phys. **140**, 18A515 (2014).
[19] S. Raghunathan and M. Nest, J. Chem. Theory Comput. **7**, 2492 (2011).
[20] F. Aryasetiawan and O. Gunnarsson, Phys. Rev. B **66**, 165119 (2002).
[21] Y. Li and C. Ullrich, J. Chem. Phys. **129**, 044105 (2008).
[22] C. Verdozzi, Phys. Rev. Lett. **101**, 166401 (2008).
[23] D. J. Carrascal and J. Ferrer, Phys. Rev. B **85**, 045110 (2012).
[24] M. Farzanehpour and I. V. Tokatly, Phys. Rev. B **86**, 125130 (2012).
[25] J. I. Fuks, M. Farzanehpour, I. V. Tokatly, H. Appel, S. Kurth, and A. Rubio, Phys. Rev. A **88**, 062512 (2013).
[26] R. Baer, J. Chem. Phys. **128**, 044103 (2008).
[27] K. Capelle and V. L. Campo, Jr., Phys. Rep. **528**, 91 (2013).
[28] J. I. Fuks and N. T. Maitra, Phys. Chem. Chem. Phys., doi:10.1039/c4cp00118d.
[29] J. P. Perdew, in *Density Functional Methods in Physics*, edited by R. M. Dreizler and J. da Providencia (Plenum, New York, 1985).
[30] O. V. Gritsenko and E. J. Baerends, Phys. Rev. A **54**, 1957 (1996).
[31] D. G. Tempel, T. J. Martínez, and N. T. Maitra, J. Chem. Theory Comput. **5**, 770 (2009).
[32] P. Elliott, S. Goldson, C. Canahui, and N. T. Maitra, Chem. Phys. **391**, 110 (2011).
[33] O. V. Gritsenko, S. J. A. van Gisbergen, A. Görling, and E. J. Baerends, J. Chem. Phys. **113**, 8478 (2000).
[34] N. T. Maitra and D. G. Tempel, J. Chem. Phys. **125**, 184111 (2006).